

B. RUSSO  
G.Z. CAO 

# Fabrication and characterization of fluorine-doped thin oxide thin films and nanorod arrays via spray pyrolysis

University of Washington, Department of Materials Science and Engineering, 302 Roberts Hall,  
Box 352120, Seattle, WA 98195, USA

Received: 23 March 2007/Accepted: 11 August 2007

Published online: 6 September 2007 • © Springer-Verlag 2007

**ABSTRACT** This paper reports the synthesis and characterization of fluorine-doped tin oxide (FTO) thin films via intermittent spray pyrolysis utilizing a solution mixture of tin chloride pentahydrate and ammonia fluoride. Utilizing the same solution, nanorod arrays were fabricated via template-based growth. Uniform and crack-free FTO films over  $20 \times 20$  mm with a thickness up to 900 nm have been routinely achieved; such FTO films demonstrate electrical resistivity as low as  $2.2 \times 10^{-4} \Omega \text{ cm}$  as well as good optical transparency ranging from 75 to 85%. In addition, FTO nanorods were fabricated using template-filling methods at a temperature of 440 °C. The nanorods have a diameter of  $\sim 160$ –250 nm, appear to be comprised of small nanoparticles 5–10 nm in size, and have a resistivity value of  $4 \times 10^{-1} \Omega \text{ cm}$ .

**PACS** 81.07.-b; 73.61.-r; 81.16.Be


## 1 Introduction

Transparent conductive oxides (TCO) have become increasingly important in a large variety of applications due to demands for optically-transparent, conductive materials. Applications of these devices include thin-film solar cells [1], display devices [1], optoelectronic devices [2], polymer-inorganic composite solar cells [3], gas sensors [4], and frost-resistant surfaces [4]. A common TCO used in research and industry is tin-doped indium oxide (ITO). ITO is an n-type semiconductor where indium oxide ( $\text{In}_2\text{O}_3$ ) has been doped with tin oxide (typically on the order of 10 at. %) [5] in order to improve many of the material's properties, including its electrical conductivity [6]. ITO has several advantages over other TCOs such as superior conductivity [7] and high optical transparency [8]. In the indium–tin oxide system, there are two extrinsic sources of charge-carrying electrons. The Sn dopant, which substitutes for indium in the crystal lattice, functions as an electron donor (generating one additional electron per Sn atom). The other electron source is oxygen vacancies, whose presence functions as an electron donor generating two electrons per oxygen vacancy [9]. However, ITO experiences a reduction of electrical conductivity when exposed to oxygen at elevated temperatures ( $> 300$  °C) [7]. At

higher temperatures, oxygen in the atmosphere combines with oxygen vacancies. When the number of oxygen vacancies decreases and the number of charge carriers reduces accordingly, the electrical conductivity decreases [10]. Since many of the above-mentioned devices undergo thermal treatments, this reduction of conductivity becomes problematic. Therefore, FTO, which is much more thermally stable, is often used as an alternative to ITO.

FTO is an ideal candidate for applications requiring TCO due to its ability to adhere strongly to glass, resistance to physical abrasion, chemical stability, high optical visible transparency, and electrical conductivity [11]. In the case of FTO, fluorine (F) is doped into tin oxide where fluorine substitutes for  $\text{O}^{2-}$  and acts as an electron donor, resulting in an n-type degenerate semiconductor [6]. Fluorine is an ideal substitution for oxygen because the anionic sizes are rather similar ( $R_{\text{O}^{2-}} = 1.32 \text{ \AA}$  and  $R_{\text{F}^-} = 1.33 \text{ \AA}$ ) and the energy of the Sn–F bond ( $\sim 26.75 \text{ D}^\circ/\text{kJ mol}^{-1}$ ) is similar to that of the Sn–O bond ( $\sim 31.05 \text{ D}^\circ/\text{kJ mol}^{-1}$ ) [12]. FTO is frequently used as an alternative to ITO when chemical and electrical stability at elevated temperatures is required for device fabrication or application. FTO is more thermally stable because it does not depend on oxygen vacancies to provide charge carriers. As a result, when exposed to elevated temperatures, FTO does not experience the characteristic decrease in conductivity seen in the ITO system [6]. Additionally, as device size continues to decrease, the potential use of nanoscaled structures of these TCOs grows. Methods for fabricating metallic [13] and semiconducting [14] nanorods have already been detailed in various published works. Certain transparent conducting oxide nanorods have also been synthesized, such as  $\text{SnO}_2$  nanorods [15] and ITO nanorods [16]. In particular, the ITO nanorods were fabricated via sol–gel electrophoretic deposition as reported in our previous work [16]. However, very little to no work has been published regarding the fabrication of FTO nanorods. Via solution techniques along with template-based growth, several parameters such as doping level, nanorod diameter, and nanorod density can be controlled when fabricating TCO nanorods.

An ordered array of these transparent, conductive oxide nanorods can provide distinct advantages for devices that utilize TCO. For example, nanorod arrays provide far greater surface area (over 100 times more) than thin films and thus offer great advantages in applications where surface area

 Fax: +1-206-543-3100; E-mail: gzcao@u.washington.edu

plays a critical role. Transparent conductive oxide nanorods have been successfully used as electrodes to improve the performance of light emitting diodes [17]; as a highly selective and sensitive gas sensor capable of detecting CO, H<sub>2</sub>, O<sub>2</sub>, and NO<sub>2</sub> [18], and as lithium ion battery anodes, which achieved significantly higher than theoretical specific capacity values [19]. More recently, conductive oxides have been employed as biological and chemical sensors [20], as ultraviolet lasers that are ideal microlight sources [21], and as photodetectors [22]. Zinc oxide nanorods have also been used as high performance nanologic circuits, helping to develop the field of oxide-based nanoelectrical devices [23]. In addition, the possibility of utilizing transparent conductive oxide nanorods in both dye-sensitized solar cells and organic solar cells may help to boost device performance. This approach has already been attempted in zinc oxide systems [24, 25], but not with several other TCO material systems. Given the current intense interest in nanotechnology and energy harvesting systems, TCO nanostructures are set to make great impacts. Although transparent oxide nanorods comprised of ITO and pure tin oxide have been used in many of the applications above, FTO nanorods have not. Given additional research, it may be possible to apply the distinct advantages of FTO to many of the above-noted specific systems.

## 2 Experimental

### 2.1 Solution synthesis

Although there is a wide range of recipes for FTO synthesis [26–28], the recipe used was adopted from the work of Kawashima et al. due to its ease of fabrication and its production of consistent results [10]. The chemicals used are tin chloride pentahydrate (SnCl<sub>4</sub> × 5H<sub>2</sub>O, 10.5 g from Sigma-Aldrich) dissolved into 150 mol of ethanol (200 proof from Aaper) in a sealed container. The solution is stirred for at least 5 h until all the tin chloride pentahydrate has completely dissolved. At this point the solution will appear nearly completely clear with a very slight amount of turbidity. Simultaneously, 1.86 g of ammonium fluoride (NH<sub>4</sub>F from Fisher Scientific) is dissolved into 4.05 ml of distilled water in a sealed container. This solution is also allowed to stir until the ammonium fluoride has been fully dissolved and the solution is completely clear. After both solutions have been allowed to fully stir, the tin chloride pentahydrate solution is placed in a water bath and heated to 60 °C. Next, the ammonium fluoride solution is then admixed. The combined solution is allowed to stir overnight to ensure complete mixing, and the resulting solution is clear and stable. This solution can then be used for thin film and nanorod synthesis. The result is a solution where the fluorine doping is fixed at 20 wt. %, which is a common concentration seen in several publications [10, 26]. It has been found that at this concentration, optimal material performance in terms of resistivity can be achieved [26, 27].

### 2.2 Film synthesis

Several thin films samples were fabricated on glass slides (2.5 cm × 2.5 cm × 0.11 cm) (VWR Microslide). Film synthesis was via spray pyrolysis (the spray apparatus is a VWR Atomizer 125 ml); in this process, a reservoir of so-

lution is atomized through a nozzle with nitrogen. The nozzle was kept 10 cm above the substrate. The substrate was heated to temperatures ranging from 220 to 440 °C. The solution was deposited by compressed nitrogen, at a pressure of 0.0344 MPa, and at a rate of 0.5 ml/min. Between bursts of deposition, the temperature of the heated surface was monitored with a thermocouple and it was found that after a burst of deposition the temperature could drop by as much as 20 °C. Therefore, sufficient time (typically around 1–2 min) was allotted to allow the heated surface to return and equilibrate at the designated temperature. Through the above process films as thick as 900 nm could be successfully fabricated.

### 2.3 Nanorod synthesis

FTO nanorod arrays have also been synthesized applying the somewhat similar method used by Limmer et al. [16], who used electrophoretic deposition, and Takahashi et al., who used capillary-based techniques [29]. An anodic alumina template (Whatman 200 nm channel diameter) is adhered to a glass substrate and solution is transferred to the templates and via capillary induction or spray pyrolysis, the solution permeates the membrane. After the template has absorbed the solution and the solution has dried, the template and substrate are transferred to a hotplate at a known temperature. After several minutes, the templates and substrates are removed and allowed to cool. This procedure can be repeated to construct longer nanorods to the extent the template allows. After cooling, the substrates and templates are transferred to a bath of 40 wt. % potassium hydroxide (Fisher Scientific) dissolved in water and allowed to soak overnight. During this step, the aqueous potassium hydroxide solution chemically reacts with and removes the alumina oxide template. After the potassium hydroxide bath, the samples are transferred to a distilled water bath, allowed to soak for several hours, and are then dried and ready for examination or characterization.

### 2.4 Characterization

X-ray diffraction for the thin films and nanorod samples was performed on a Phillips 1830 diffractometer. The films and nanorod samples were observed with a JOEL JSM-7000 scanning electron microscope (SEM). Resistivity values were measured with a four-point probe digital multimeter (Fluke 8842A Multimeter).

## 3 Results and discussion

### 3.1 FTO thin films

Uniform crack-free films can be readily fabricated through the intermittent spray pyrolysis of a mixture solution of tin chloride pentahydrate in ethanol mixed with ammonium fluoride in water on glass substrate at temperatures ranging from 220–440 °C. When using a spray pressure of 0.0344 MPa, films up to 70 nm thick can be grown per minute. Film thicknesses of up to 900 nm have been achieved. XRD spectroscopy revealed that FTO films grown at 400 °C consist of FTO with only trace amounts of potential impurity. Figure 1(a) shows an XRD pattern of a thin film deposited at 400 °C; the diffraction peaks can be indexed to SnO<sub>2</sub> phase [1, 10, 26]. No appreciable peak shift can be observed,

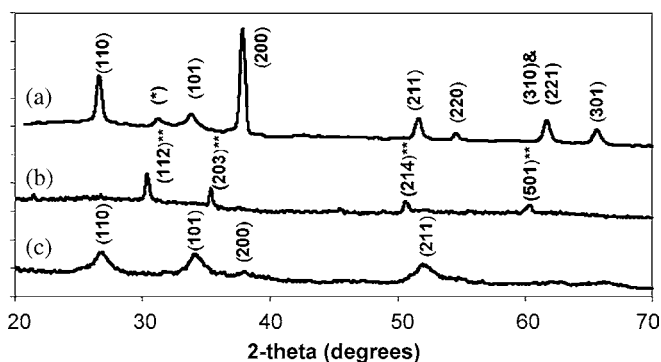


**FIGURE 1** XRD pattern for FTO: *a* thin film processed at 440 °C (\* peak may be a result of tin chloride residue), *b* thin film processed at 220 °C (\*\* indicates tin chloride), *c* FTO nanorods in alumina membrane

which is reasonable considering the doping level is relatively small for this system and the anionic radii are rather similar ( $R_{O^{2-}} = 1.32 \text{ \AA}$  and  $R_{F^-} = 1.33 \text{ \AA}$  with CN = 6) [12]. Figure 1(b) shows an XRD of a thin film deposited at 220 °C; at this temperature, crystalline tin oxide cannot form. This film resulted in a combination of tin chloride and amorphous tin oxide. The formation of amorphous tin oxide at low processing temperatures has been established in other published works [30].

Figure 2 displays the optical transmission range for several samples; the first two samples were fabricated at low temperatures (220 °C and 320 °C). Figure 2 also shows the transmission range for a FTO sample synthesized at 440 °C via spray pyrolysis. Between 450 and 800 nm the transmission varies between 75 and 85%, with a peak transmission of 93% around 650 nm. This value is comparable (and in certain ranges is superior) to literature values [10]. In addition, Fig. 2

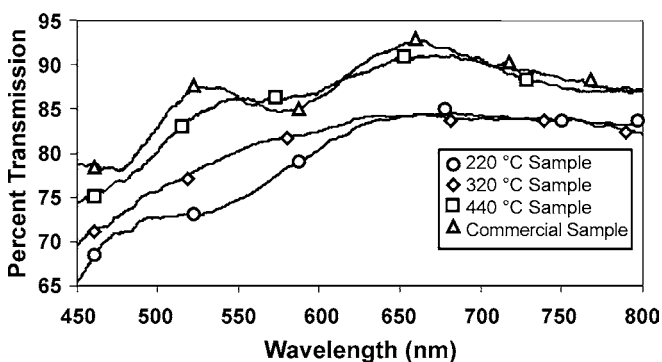


**FIGURE 2** Optical transmittance for sample processed at 220 °C, sample processed at 320 °C, sample processed at 440 °C, and commercial FTO sample (for reference)

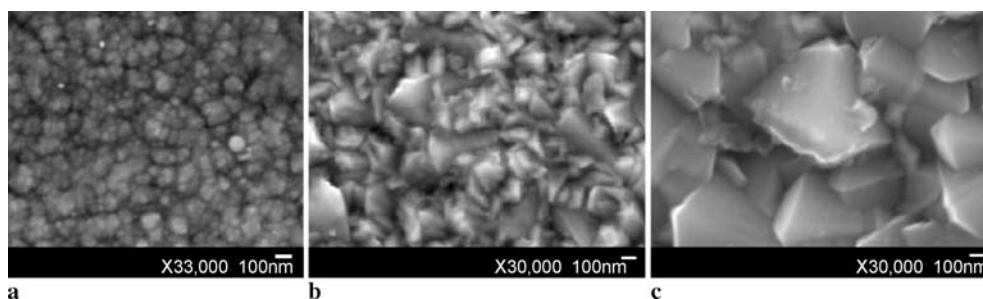


**FIGURE 3** Film surface morphology for *a* film processed at 220 °C, *b* FTO film processed at 320 °C, and *c* FTO film processed at 440 °C

displays the transmission range for a commercial sample of FTO (Solaronix TCO22-15) for the purpose of a reference. Between 450 and 800 nm the transmission varies between 80 and 85% with a peak transmission of 91% near 650 nm. It is clear that as the processing temperature decreases the optical transmittance of the samples decreases. At the lower temperature, greater concentrations of impurities are present, which results in less transparent samples. In addition, grain-boundary scattering [31] due to the presence of smaller grains and the presence of voids in the film also decreases the optical transmittance. As the grain size increases due to higher deposition temperatures (see Fig. 3), there is notably less grain-boundary scattering. For the range of wavelengths examined, the commercial FTO sample has an average transmission of 87%, while the in-house synthesized FTO sample has an average transmission of 86%.

Figure 3 displays SEM micrographs of the fabricated thin films. Figure 3a shows the surface morphology of the thin films deposited at 220 °C. As the figure shows, the film is comprised of many small uniaxial grains with a grain size around 70–100 nm. Although the grains do not appear to be well packed, there are no visible cracks in the film. Figure 3b displays the surface morphology of a film deposited at 320 °C. The sample has a grain size of 100–200 nm with a few larger grains (~250 nm) interspersed. Figure 3c shows the surface morphology of a FTO film deposited at 440 °C. The grain size is 200–300 nm, which is considerably larger than that in film grown at 220 °C or 320 °C. Clearly, the grain size in films increases with the increasing deposition temperature. Furthermore, the grains in the film deposited at 440 °C have developed much more well-defined facets than the grains in the 220 °C film, implying that the 440 °C film possesses much better crystallinity. This is consistent with the XRD results, given the signal-to-noise ratio of the respective samples. The surface roughness also noticeably increases with the increased deposition temperature, which can be ascribed to the increased crystalline grain size and the better-developed facets.

Figure 4a displays the cross-section of a thin film fabricated at 220 °C. The thickness of this sample is 300–400 nm. For this low temperature sample, the film is comprised of small grains; in addition, the grains are not dense due to the presence of voids. Figure 4b displays the cross-section of FTO film deposited at 440 °C. The thickness is ~900 nm and is consistent throughout the sample. The cross-section image also clearly showed that the film is dense, i.e., no voids. The film in Fig. 4c (a 1.5× digitally magnified image of Fig. 4a) has a columnar structure (some of the columns are outlined in black) with the grains smaller near the substrate

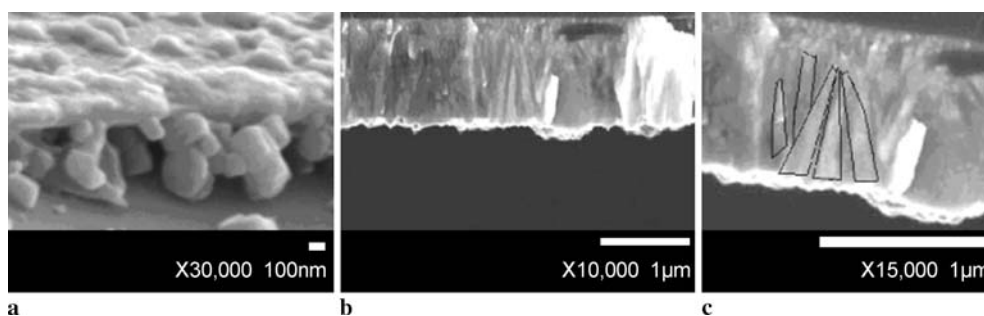


**FIGURE 4** FTO thin film cross-section for samples fabricated at **a** 220 °C and **b** 440 °C. **c** 440 °C sample digitally magnified 1.5× and outlined to reveal column structure

surface and gradually becoming larger towards the surface. Such columnar structure is observed in films deposited at high temperatures but not in films grown at low temperatures. At lower deposition temperatures, there is not sufficient energy to promote the desired surface diffusion and thus secondary nucleation occurs, resulting in the formation of small uniaxial-grained microstructures. However, at higher deposition temperatures, there is sufficient energy to promote surface diffusion and thus no secondary nucleation occurs, leading to the columnar growth. The increased grain size from the substrate surface to the film surface can be easily ascribed to evolution selection growth. Such columnar structured films are often observed in many systems ranging from copper to aluminum oxide where they have been deposited via several different methods [32].

Finally, the film resistivity as a function of thermal deposition temperature (220–440 °C) was tested with a four-point probe test. Figure 5 displays the resistivity values; as can be seen, the films are all conductive and as the deposition temperature increases the resistivity values decrease. This decrease is due to the formation of FTO at higher temperatures, which is not possible at a temperature of 220 °C. These results

are in agreement with the XRD spectrum shown in Fig. 1. The samples fabricated at 440 °C have the best performance with a resistivity value of  $2.2 \times 10^{-4} \Omega \text{ cm}$  and a sheet resistance value of  $2.38 \Omega/\text{square}$  for a film  $\sim 900 \text{ nm}$  thick. This is one of the better-reported values in literature with literature values ranging from  $5.8 \times 10^{-4} \Omega \text{ cm}$  [1] to  $2.0 \times 10^{-4} \Omega \text{ cm}$  [33] for FTO fabricated via spray pyrolysis. As the spray pyrolysis temperature increases, the crystallinity of the thin film also increases (as seen in the figures above). This increase in grain size allows for superior charge mobility, thereby improving the electrical performance [12].

### 3.2 FTO nanorods

Figure 6 displays SEM images of the FTO nanorods fabricated at 440 °C. The nanorods varied in size between  $\sim 160$  and  $\sim 250 \text{ nm}$ . The reason for the variation is inconsistencies in pore diameter and shape (and occasionally merged pores) due to the manufacturing of these templates. Some of these nanorods display a minimal amount of shrinkage (around  $\sim 10\%$ ) compared to the original template diameter. In addition, the nanorods are rather straight and express little

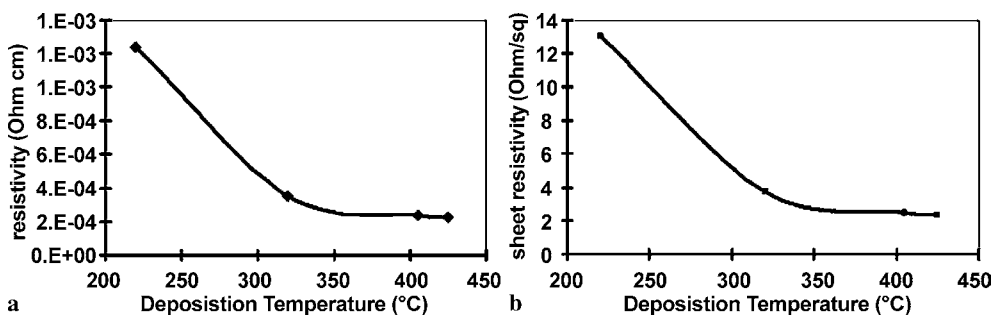


**FIGURE 5** Resistivity and sheet resistivity of FTO films as a function of spray deposition temperature

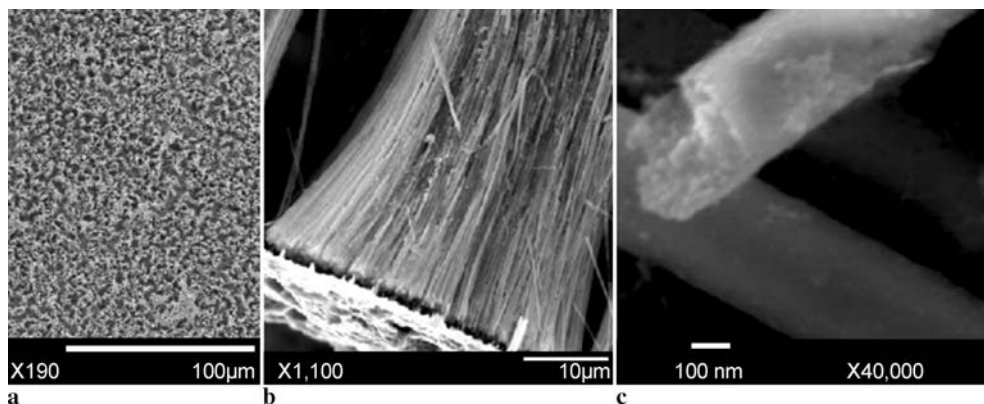


**FIGURE 6** SEM micrographs of FTO nanorods grown in 200 nm alumina template: **a** low magnification field of FTO nanorods **b** FTO nanorods in a standing array, **c** high magnification image of one nanorod

to no curvature. The aspect ratio for these nanorods is  $\sim 250$ – $300$ . Figure 6a shows the relatively large arrays of nanorods that can be fabricated, while Fig. 6b shows a higher magnification image of the nanorod array. In this particular image, the highly ordered nature of the array is evident. Lastly, Fig. 6c shows a high magnification image of a broken nanorod. The nanorods appear to be comprised of many small particles on the order of 5–10 nm. They are relatively well packed and, in general, do not form large voids.

Given the nature and uses of FTO, approximating the resistivity of the FTO nanorods was deemed valuable. A sample was synthesized in an anodic alumina membrane and pyrolyzed at 440 °C so as to mimic the conditions that result in high quality thin films. The resulting product is a composite structure of FTO nanorods within an alumina membrane. XRD (Fig. 1c) was performed in order to verify the existence of FTO that compares to the spectra of FTO thin films (fired at 440 °C). Next, electrodes were placed on either side of the membrane with silver adhesive and leads were attached so that a resistivity test could be conducted. The resistance was 1.5  $\Omega$  after removing the resistance that was a result of the wires and adhesive (this resistance was established by measuring the resistance of just the wires and silver past adhesive without the membrane). This data was used to calculate an estimated resistivity for the nanorod samples based upon the fact that the electrode area is 0.08 cm<sup>2</sup> and the density of the nanorods is 10<sup>9</sup> units/cm<sup>2</sup>, with the length of the rods equal to the thickness of the membrane (60  $\mu$ m) and the diameter of the rods equal to the membrane pore size (140 nm). Based upon these values, the calculated bulk resistivity for the nanorods is  $4 \times 10^{-1} \Omega$  cm.

Due to the nature of the test, the results are not likely to be identical to the thin film measurements. However, such tests do allow us to verify the conductive nature of the rods as well as to estimate the general nanorod resistivity. The difference between values could be the result of several factors. Firstly, it is clear that not all the nanorods survive the template removal process. Some rods are broken while others are sheared off entirely. Therefore, broken rods that do not act as a conductive pathway will result in a higher calculated resistivity than is actually true. Additionally, it is possible that not all the membrane pores are filled, resulting in a similar error to the one mentioned previously. Also, as was seen in Fig. 3, the film is polycrystalline and so it is safe to assume that the nanorods are also polycrystalline in nature. Thus, grain-boundary scattering may have an impact on nanorod performance.

#### 4 Conclusions

FTO thin film synthesis via spray pyrolysis can be a cost-effective method for producing high quality films. Thin films were produced at a wide range of temperatures; the optimal temperature was 400–440 °C where highly conductive, transparent, and crack-free films could be produced. Films produced via this technique have resistivities as low as  $2 \times 10^{-4} \Omega$  cm and optical transparencies around 85%. With the same solution, nanorod arrays of FTO were produced. At

this time, there is no other known publication concerning the successful fabrication of FTO nanorods. The FTO nanorods have a resistivity of  $4 \times 10^{-1} \Omega$  cm.

**ACKNOWLEDGEMENTS** We acknowledge the Air Force Office of Scientific Research (AFOSR-MURI, FA9550-06-1-032) and the National Science Foundation (DMI-0455994) for partial financial support. BR would like to acknowledge the NSF-IGERT fellowship from the Center for Nanotechnology at UW for its fiscal support, and Robert Smith for assistance in constructing the apparatus utilized in the research. Lastly, BR would like to acknowledge the help received from Tammy Chou and Qifeng (Jeff) Zhang during the course of this research.

#### REFERENCES

- 1 T. Fukano, T. Motohiro, *Sol. Energ. Mater. Sol. Cells* **82**, 567 (2004)
- 2 N.R. Lynam, in *Proceedings of the Symposium on Electrochromic Materials*, vol. 90–92, ed. by M.K. Carpenter, D.A. Corrigan. (The Electrochemical Society, Pennington, 1990), p. 201
- 3 Q. Qiao, J. Beck, R. Lumpkin, J. Pretko, J.T. Mcleskey Jr., *Sol. Energ. Mater. Sol. Cells* **90**, 1034 (2006)
- 4 A.N. Banerjee, S. Kundoo, P. Saha, K.K. Chattopadhyay, *J. Sol-Gel Sci. Technol.* **28**, 105 (2003)
- 5 H. Fujiwara, S. Otsuka-Yao-Matsuo, N. Ono, *Appl. Phys. A* **71**, 609 (2000)
- 6 S. Ngamsinlapasathiana, T. Sreethawongb, Y. Suzukia, S. Yoshikawa, *Sol. Energ. Mater. Sol. Cells* **90**, 2129 (2006)
- 7 G.R.A. Kumara, S. Kaneko, A. Konno, M. Okuya, K. Murakami, B. Onwona-Agyeman, K. Tennakone, *Prog. Photovoltaics Res. Appl.* **14**, 643 (2006)
- 8 T. Fukano, T. Motohiro, T. Ida, H. Hashizume, *J. Appl. Phys.* **97**, 084314 (2005)
- 9 S.N. Luo, A. Kono, N. Nouchi, F. Shoji, *J. Appl. Phys.* **100**, 113701 (2006)
- 10 T. Kawashima, H. Matsui, N. Tanabe, *Thin Solid Films* **445**, 241 (2003)
- 11 G.C. Morris, A.E. McElnea, *Appl. Surf. Sci.* **92**, 167 (1996)
- 12 C. Agashe, S.S. Major, *J. Mater. Sci.* **31**, 2965 (1996)
- 13 P. Shao, G. Ji, P. Chen, *J. Membr. Sci.* **255**, 1 (2005)
- 14 Y.J. Kim, H. Shang, G.Z. Cao, *J. Sol-Gel Sci. Technol.* **38**, 79 (2006)
- 15 W. Wang, C. Xu, X. Wang, Y. Liu, Y. Zhan, C. Zheng, F. Songa, G. Wanga, *J. Mater. Chem.* **12**, 1922 (2002)
- 16 S.J. Limmer, S.V. Cruz, G.Z. Cao, *Appl. Phys. A* **49**, 421 (2004)
- 17 J.K. Kim, J.Q. Xi, H. Luo, J. Cho, C. Sone, Y. Park, E.F. Schubert, *Proc. SPIE* **5941**, 91 (2005)
- 18 H. Hui, O.K. Tan, Y.C. Lee, T.D. Tran, M.S. Tse, X. Yao, *Appl. Phys. Lett.* **87**, 163 123 (2005)
- 19 Y. Wang, J. Yang Lee, *J. Phys. Chem. B* **108**, 17832 (2004)
- 20 Y. Cui, Q. Wei, H. Park, C.M. Lieber, *Science* **293**, 1289 (2001)
- 21 M.H. Huang, S. Mao, H. Feick, H. Yan, Y. Wu, H. Kind, E. Weber, R. Russo, P. Yang, *Science* **292**, 1897 (2001)
- 22 J. Wang, M.S. Gudiksen, X. Duan, Y. Cui, C.M. Lieber, *Science* **293**, 1455 (2001)
- 23 W.I. Park, J.S. Kim, G.C. Yi, H.J. Lee, *Adv. Mater.* **17**, 1393 (2005)
- 24 M. Law, L.E. Greene, J.C. Johnson, R. Saykally, P. Yang, *Nature Mater.* **4**, 455 (2005)
- 25 P. Charoensirithavorn, S. Yoshikawa, *Mater. Res. Soc. Symp. Proc.* **974**, CC07, (2007)
- 26 E. Elangovan, K. Ramamurthi, *Appl. Surf. Sci.* **249**, 183 (2005)
- 27 S. Shanthi, C. Subramanian, P. Ramasamy, *Mater. Sci. Eng. B* **57**, 127 (1999)
- 28 E. Shanthi, A. Banerjee, V. Dutta, K.L. Chopra, *J. Appl. Phys.* **53**, 1615 (1982)
- 29 K. Takahashi, Y. Wang, K. Lee, G.Z. Cao, *Appl. Phys. A* **82**, 27 (2006)
- 30 A. Gupta, D.K. Pandya, S.C. Kashyap, *Japan. J. Appl. Phys.* **43**, L1592 (2004)
- 31 S. Shanthia, H. Anurathab, C. Subramaniana, P. Ramasamy, *J. Cryst. Growth* **194**, 369 (1998)
- 32 J.A. Thornton, *Ann. Rev. Mater. Sci.* **7**, 239 (1977)
- 33 R. Chandrasekhar, K.L. Choy, *J. Cryst. Growth* **231**, 215 (2001)